*Istraživanja i projektovanja za privredu*
*ISSN 1451-4117*
*DOI:10.5937/jaes0-61710*
*www.engineeringscience.rs*

iipp publishing

***Journal of Applied Engineering Science***
*Original Scientific Paper,*
*Volume 24, Number 4, Year 2026,*
*No 1358, pp 618-635*

# *NUMERICAL AND DYNAMIC ANALYSIS OF CRANKPIN LOADS ON A MULTI-CYLINDER DIESEL ENGINE*

***Djamel Mazari[1]*, Soussa Abdelhalim[2], Khadidja Boualem[2], Mustapha Bordjane[2]***

*[1]University of Ibn Khaldoun-Tiaret, Faculty of Applied sciences, Department of Mechanical Engineering, Tiaret, Algeria*
*[2]University of Sciences and Technology Mohamed Boudiaf-Oran, Faculty of Mechanical Engineering, Department of Mechanical Engineering, Oran, Algeria*
**mustapha.bordjane@univ-usto.dz*

*The continuous increase in the specific power of diesel engines raises dynamic loads on the crankpin, reducing its fatigue life and bearing reliability. Although numerous studies have addressed the mechanical behavior of these components, few have examined how the connecting rod dynamic model affects the loads on the crankpin and the resulting stress distribution. This study develops an algorithm to analyze the dynamic behavior of the crankshaft-connecting rod system of a six-cylinder in-line diesel engine (MIDR 0635 40 M/3). The original contribution of this work is a systematic, quantitative comparison of crankpin loads from two distinct models: the two-lumped-mass connecting rod model (simplified model, neglecting the actual moment of inertia of the connecting rod) and the effective connecting rod model (with distributed inertia, preserving mass, center of gravity, and actual moment of inertia). In a second step, a finite element method (FEM) numerical simulation is carried out on the crankpin using Abaqus software. Two strength criteria are applied: the Von Mises criterion for equivalent stress evaluation, and the critical loading condition at top dead center (TDC), corresponding to the maximum combustion pressure (Pmax = 187.55 × 10 $^{-3}$ MN). The results show that the simplified model overestimates inertia forces and the shock parameter, with deviations reaching 6.6% compared to the effective model. The numerical Von Mises stresses obtained (128.9 MPa) are in good agreement with the analytical values (140.20 MPa), both below the material yield limit (560 MPa), confirming the validity of the proposed approach.*

*Keywords: modelling, crankshaft, dynamic loading, inertia, finite elements, Von Mises stresses, diesel engine*

## *HIGHLIGHTS*

- Two models are used to evaluate the inertial effects on the dynamic loading of multi-cylinder diesel engine crankpin, namely, the simplified and the effective connecting rod models;
- An algorithm is developed to analyze the dynamic behavior of the crankshaft-connecting rod system;
- Numerical simulation using Abaqus software, is carried out on the crankpin of a multi-cylinder diesel engine;
- Tow hypotheses are used to evaluate material strength and calculate the different stresses caused by loads on the crankpin;

## *NOMENCLATURE*

| | | | |
|---|---|---|---|
| $\omega$ | Angular velocity of crankshaft [rad/s] | m | Total reciprocating mass ($m_{pg}$+$m_{cbe}$) [kg] |
| $\beta$ | Connecting rod oscillation angle [rad] | $m_c$ | Connecting rod mass [kg] |
| $\omega_b$ | Connecting rod oscillation velocity [rad/s] | $m_{pg}$ | Piston group mass ($m_p$+$\sum m_r$+$m_{pp}$) [kg] |
| $\varepsilon_b$ | Connecting rod oscillation acceleration [rad/s$^2$] | $m_{cse}$ | mass of connecting rod small end (1/3) mc [kg] |
| $\lambda$ | Ratio crankshaft radius/connecting rod length | $m_{cbe}$ | mass of connecting rod big end (2/3) mc [kg] |
| $L_G$ | Distance (big end/connecting rod) centers [mm] | $m_r$ | Rings mass [kg] |
| $\varphi$ | Crank angle of the crankshaft (CA) [deg] | $m_p$ | Piston mass [kg] |
| $P_\Sigma$ | The sum of gas pressure and inertia forces [MN] | $m_{pp}$ | Mass of piston pin [kg] |
| N | Side thrust force [MN] | r | Crank radius [mm] |
| T | Tangential load [MN] | D | Cylinder bore [mm] |
| Z | Normal load [MN] | $S_p$ | Piston head area ($\pi D^2/4$) [mm$^2$] |
| $P_g$ | Force due to the combustion gas pressure [MN] | $a_N$ | Normal acceleration [m/s$^2$] |
| $P_j$ | Reciprocating parts inertia forces [MN] | $\lambda$=r/L | Dimensionless mechanism characteristic |

| | | | |
|---|---|---|---|
| $p_{cyl}$ | Cylinder gas pressure [MPa] | BDT | Bottom dead center |
| $P_k$ | Counter pressure [MPa] | TDC | Top dead center |
| $P_{ko}$ | Centrifugal force [MN] | Q | Loads [MN] |

## 1 Introduction

The crankshaft is one of the most characteristic and most heavily loaded components of an internal combustion engine. Its main function is to transform the reciprocating motion of the pistons, generated by gas combustion in the combustion chamber, into continuous rotary motion that drives many mechanical systems such as generators, pumps and compressors [1]. This transformation involves complex and variable mechanical loads, the mastery of which directly conditions the durability and reliability of the engine.

Due to fluctuations in engine speed during the operating cycle, the crankshaft is subjected to inertial torques whose amplitude depends on the geometry and distribution of moving masses. The rapid rotation of the crankshaft about its fixed axis generates considerable inertial forces acting on the main bearings, significantly increasing contact stresses. These undesirable phenomena are mitigated when the inertial forces of the rotating masses are balanced, which justifies the importance attached to the optimization of mass distribution in the design of modern crankshafts [2, 3].

In internal combustion engines, two main sources of loading act on the crankshaft: the gas pressure forces from combustion and the inertial forces of the reciprocating masses. These two sources simultaneously generate bending and torsional stresses in the shaft [4]. The connecting rod, the linking element between the piston and the crankshaft, transmits the gas pressure to the crankpin as two components: a tangential force, which generates the engine torque, and a radial force, causing crankshaft bending. This results in a three-dimensional cyclic stress state, which generally peaks under maximum combustion pressure, approximately 5° to 10° after top dead centre (ATDC) [7].

Of the various bearings of the diesel engine, the connecting rod big-end and small-end bearings as well as the crankshaft main bearings are the most heavily loaded. They are subjected to varying loads and speeds throughout the engine cycle. The amplitude and direction of the resulting forces acting on these bearings depend on three factors: the gas pressure forces, the inertial forces of the reciprocating masses, and the centrifugal forces created by the connecting rod big end at the crankpin level [5, 6]. The crankpin, the junction zone between the connecting rod and the crankshaft, thus constitutes the most critical region of the system, both in terms of static stress and fatigue life [8, 9].

The dynamic modelling of the slider-crank mechanism is a fundamental step in evaluating loads on the crankpin. In industrial practice, the most commonly used model is the simplified two-lumped-mass model with two masses, which distributes the connecting rod mass between the small-end (1/3 mc) and the big-end (2/3 mc). Although this model is simple to implement, it introduces a systematic error in the connecting rod's moment of inertia, leading to incorrect predictions of rotational inertial torques and, consequently, to a poor evaluation of internal forces and engine dynamics [10]. The effective connecting rod model, on the other hand, treats the connecting rod as a rigid body with distributed inertia, simultaneously preserving its total mass, the position of its centre of gravity and its actual moment of inertia, thus offering a physically more rigorous representation.

Although several studies have investigated the mechanical behaviour of internal combustion engine crankshafts, few have systematically and quantitatively analysed the influence of the connecting rod dynamic model on the loads applied to the crankpin and on the stresses developed within it, particularly for industrial multi-cylinder diesel engines. The present study fills this gap by proposing a detailed comparison between the simplified model and the distributed-mass model, applied to a six-cylinder in-line diesel engine (type MIDR 0635 40 M/3). The loads thus obtained are then used as input data for a three-dimensional finite element numerical analysis performed in Abaqus, enabling the evaluation of stress distribution, safety factor, and the operating conditions of the crankpin bearing. This integrated approach serves as a tool for the sizing and optimization of diesel engine crankshafts subjected to severe dynamic loading.

### 1.1 Literature review

Crankshafts of internal combustion engines, and particularly their crankpins, have been the subject of numerous studies addressing various issues such as mechanical loads, lubrication, dynamic performance and fatigue life. These studies have been conducted using complementary approaches — theoretical, numerical and experimental — reflecting the inherent complexity of analysing these components subjected to severe cyclic loadings. The present review is organized chronologically to highlight the evolution of methods and contributions in this field.

Among the foundational contributions, Shiao and Moskwa [10] highlighted the dynamic errors introduced by the two-lumped mass connecting rod model compared to the actual connecting rod model. Their work demonstrates that the conventional analytical method for estimating the moment of inertia remains approximate and leads to incorrect predictions of internal forces and engine dynamics. This observation constitutes one of the starting points of the present study. Subsequently, Montazersadgh and Fatemi [11, 12] carried out dynamic finite element simulations on single-cylinder four-stroke crankshafts, establishing that any structural optimization requires a rigorous evaluation of the combined bending and torsional loads. They recommend increasing the fillet radius and introducing compressive residual stresses at the crankpin level to improve fatigue resistance.

Parejiya et al. [4] demonstrated, based on three-dimensional models, that the highest stress levels systematically concentrate at the crankpin/web and journal-web intersections, potentially reaching critical values if sizing is not rigorously controlled. Kumar et al. [1] complemented this analysis by distinguishing two critical loading positions for the crankpin: the maximum bending position at bottom dead centre (BDC), likely to induce bending failure, and the maximum torsion position, located between 30° and 40° from BDC for diesel engines, exposing the crankpin to shear failure. Mrdja et al. [2] proposed an original approach for estimating the overall engine inertia from transient regime tests combined with thermodynamic cycle analysis, showing that dynamically estimated inertia is slightly higher than static values, with deviations depending on the engine speed ramp.

Moon [14] established that the operating clearance and lubricant temperature play a determining role in maintaining a sufficient hydrodynamic film at the crankpin bearing of a marine two-stroke diesel engine, and that optimizing these parameters prevents direct metal-to-metal contact. Sun et al. [15] analyzed the load and lubrication performance of connecting rod and main bearings at different operating conditions, combining dynamic methods and finite elements. Their results show that translational and rotational inertial forces increase with engine speed, but counteract the cylinder pressure at TDC, which reduces the maximum load on the connecting-rod bearing at high speeds — a result directly consistent with the multi-speed polar diagrams obtained in the present study. Nikolić et al. [13] developed a computer program for generating polar load diagrams for all crankshaft bearings, recommending the use of optimized counterweights to reduce the amplitude of bearing loads and improve overall engine reliability.

Cihan [16] conducted a systematic numerical study on the influence of speed and pressure on Von-Mises stresses and nodal deformations of the crankshaft, confirming that stress concentrations at the crankpin journal constitute the most critical region in a multi-cylinder engine. Sumardiyanto and Susilowati [17] examined the influence of diesel engine vibrations on crankpin bearing wear, showing that failures result mainly from insufficient lubrication or the presence of contaminants — combustion residues, water vapor, abrasive particles — leading to progressive erosion of the bearing walls.

More recent work has brought significant and complementary contributions to this field. Sun et al. [18] confirmed in detail that the maximum load on the connecting rod bearing decreases with increasing engine speed, a result consistent with the multi-speed polar diagrams of the present study. Solangi et al. [19] and Azzawi et al. [20], in 2023, both conducted FEM analyses of diesel crankshafts using ANSYS, confirming that maximum stresses concentrate at the crankpin and fillet zones, with safety factors calculated according to a methodology directly comparable to that adopted here. In the same year, Yin et al. [21] developed a tribo-dynamic model for the connecting rod big-end bearing, integrating elastic deformation and thermal effects of the lubricant. Their simulations, validated on a full-scale engine test bench, reveal non-uniform axial wear absent from rigid contact models, thus highlighting the limitations of the rigid contact hypothesis adopted in the present study and identifying a path for future improvement.

In 2024, Jayanthan et al. [22] calculated the radial and tangential components of the force on the crankpin using ADAMS simulation coupled with FEM analysis, confirming that this force reaches its peak at approximately 130° crank angle — a result consistent with the polar diagrams of the present study. More recently, in 2025, Chmielowiec et al. [23] proposed a complete three-dimensional model of the inertia force field on a moving connecting rod, demonstrating that this 3D model provides significantly different results from those of the two-lumped mass model, particularly for connecting rods with asymmetric geometry. This finding directly reinforces the conclusions of the present study on the deviations between the two connecting rod models, notably on the lateral load component (N). From a complementary perspective, Chen et al. [24] developed a fatigue life prediction method for crankshafts integrating the influence of rotational speed by genetic algorithm, providing a valuable predictive dimension for interpreting the results at the different analyzed speeds. Finally, recent research on marine diesel engine crankshafts has proposed a dedicated Abaqus plugin for parametric modelling and bending analysis with experimental validation [25], offering an advanced numerical methodology complementary to classical analytical approaches.

The literature review highlights several gaps that the present study seeks to fill. On the one hand, most of the work focuses on single-cylinder engines, without considering the coupling effects between cylinders specific to multi-cylinder engines. On the other hand, comparisons between connecting rod models remain rare and are rarely coupled with a complete FEM numerical analysis on a real industrial engine. The present study provides a direct response to these gaps by proposing an integrated approach — dynamic calculation algorithm, quantified comparison of the two connecting rod models, and three-dimensional numerical simulation in Abaqus — applied to a six-cylinder in-line industrial diesel engine (MIDR 0635 40 M/3).

## 2 Materials and methods

### 2.1 Dynamic analysis

To simplify the analysis, it is assumed that the engine runs at a constant crankshaft speed, and gravitational friction forces can be neglected compared to dynamic force effects. Friction force is relatively low compared to other forces [26]. Friction forces in diesel engine bearings, although real, typically represent less than 5 to 8% of the pressure and inertial forces at the operating speeds studied (1400–2200 rpm). This approximation is consistent with the approach adopted by Parejiya et al. [4] and Kumar et al. [1]. The force applied to the piston head, according to the law of force decomposition, transmits a force to the connecting rod and a force that tends to press the piston against the cylinder wall (see Fig.1). This force itself is divided into a tangential force, tangent to the circumference of rotation, and a normal force, perpendicular to it. The tangential force, called the driving effort, drives the engine; it varies with the

piston's position, being zero at TDC, reaching a maximum, and returning to zero at BDC. The normal force tends to press the crankshaft against the bearings. This force is also continuously variable. During the expansion stroke, the gas pressure gradually decreases and theoretically ceases to act at BDC.

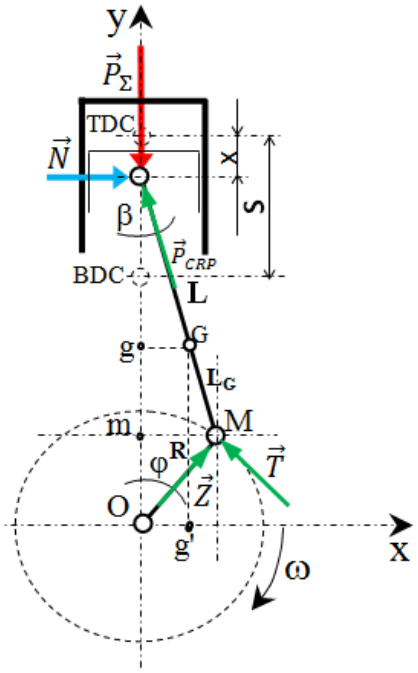


Fig. 1. Crank mechanism loads

The connecting rod is one of the most heavily stressed components in an internal combustion engine. While various modelling approaches exist in the literature, the most common industrial method is the simplified model, which treats the connecting rod as a rigid bar with two lumped masses – one reciprocating and one rotating [27, 28]. Although this model simplifies dynamic analysis, it inherently alters the actual moment of inertia of the connecting rod. This deviation leads to inaccurate predictions of internal forces and overall engine dynamics. Consequently, it is essential for designers to rigorously evaluate the magnitude of these errors when utilizing the simplified model to avoid misestimating dynamic loads [10].

### 2.2 Effective connecting rod model

In this model, the connecting rod is modeled as a rigid body with mass distributed along its length to match the mass, center of mass location, and moment of inertia of the effective rod. The forces from the piston act on the small end of the connecting rod, while the reaction from the crankshaft acts on the big end. Gravity forces and longitudinal inertia forces of the connecting rod act on its center of mass [10], Fig.1. Loads on the piston and crankpin are specified by:

$$N = P_\Sigma.\tan\beta + \frac{(I_{bG} + m_b L_G^2).\varepsilon_b}{L\cos\beta} \quad (1)$$

$$T = \frac{P_\Sigma.\sin(\varphi+\beta)}{\cos\beta} - \frac{(I_{BG} + m_b L_G^2)\cos\varphi\,.\varepsilon_b}{L\cos\beta} - m_b(\ddot{y}_G\cos\varphi - \ddot{x}_G\sin\varphi) \quad (2)$$

$$Z = \frac{P_\Sigma\cos(\varphi+\beta)}{\cos\beta} - \frac{(I_{bG} + m_b L_G^2).\sin\varphi\,.\varepsilon_b}{L\cos\beta} + m_b(\ddot{y}_G\cos\varphi + \ddot{x}_G\sin\varphi) \quad (3)$$

Where; $\beta = \sin^{-1}(\lambda\sin\varphi)$, $\omega_b = \omega\lambda\cos\varphi$, $\varepsilon_b = \lambda\omega^2(\lambda^2 - 1)\sin\varphi$,
$\ddot{x}_G = -R\omega^2\sin\varphi - \varepsilon_b L_G\cos\beta + \omega_b^2 L_G\sin\beta$, $\ddot{y}_G = -R\omega^2\cos\varphi - \varepsilon_b L_G\sin\beta - \omega_b^2 L_G\cos\beta$, $P_\Sigma = P_g + P_j$,
$P_g = (p_{cyl} - p_k).S_p$ and $P_j = -m.j$

### 2.3 Two-Lumped masses connecting rod model

This approach assumes that two lumped masses replace the mass of the connecting rod; the reciprocating part "$m_{cse}$" is fully located at the piston gudgeon-pin axis and added to the reciprocating masses, and the rotational part "$m_{cbe}$" is fully located at the crank journal axis and added to the rotational masses. Otherwise, in this model, the connecting rod is divided into reciprocating and rotating masses so that the distributed connecting rod mass is replaced by two lumped masses, each one positioned at one end of a stem or rod with negligible mass. The manufacturers of the connecting rod specify the values of these two masses. The following three equations must be satisfied to make the simplified connecting rod model equivalent to the effective connecting rod model.

$$m_c = m_{cbe} + m_{cse} \quad (4)$$

$$m_{cbe}L_1 = m_{cse}L_2 \quad (5)$$

$$J_c = m_{cbe}L_1^2 + m_{cse}L_2^2 + J_f \quad (6)$$

Satisfaction of equation (4) indicates that the connecting rod's total mass is conserved. While verifying equation (5) ensures that the center of mass position is preserved. Generally, the moment of inertia error ($J_f$) in equation (6) is ignored for a typical connecting rod (though it is not actually zero) [29]. The primary advantage of the simplified two-lumped-mass model lies in the simplicity of its system of dynamic equations. However, because the moment of inertia differs from the actual model, it yields accurate lonfitudinal inertial forces but inaccurate rotational inertial torques. These inaccuracies can lead to suboptimal engine design, negatively affecting overall balance and service life [10]. Using this simplified model, the main loads are given by:

$$N = P_\Sigma \tan\beta \quad (7)$$

$$T = P_\Sigma \frac{\sin(\varphi+\beta)}{\cos\beta} \quad (8)$$

$$Z = P_\Sigma \frac{\cos(\varphi+\beta)}{\cos\beta} \quad (9)$$

The centrifugal inertia forces and the total load on the crankpin are given by:

$$P_{k0} = m_{cbe}.a_N = m_{cbe}.\omega^2.R \quad (10)$$

$$Q = \sqrt{T^2 + (Z - P_{k0})^2} \quad (11)$$

### 2.4 Solution procedure of dynamic analysis

By applying the fundamental principle of dynamics to the connecting rod-crank mechanism, a complete model can be developed for each engine cylinder, enabling numerical simulation of the dynamic evolution of an engine cycle over its four strokes. The approach adopted in the present study relies on a sequential two-step modelling approach: first, the side thrust force (N) and the internal forces of the system are calculated using the effective connecting rod model, which faithfully integrates the actual inertia of the connecting rod — total distributed mass, exact centre of mass position and actual moment of inertia. These same forces are then recalculated using the simplified connecting rod model, which represents the connecting rod by two lumped masses at the ends of a massless rod: a rotating mass linked to the crankpin and a reciprocating mass connected to the piston pin axis. The systematic comparison of the results from the two models over the entire engine cycle makes it possible to highlight and quantify the dynamic deviations between them, thus constituting the main original contribution of this work.

The core strategy of the code involves defining the necessary parameters to evaluate the engine configuration. Common inputs (thermodynamic data, engine type, geometric parameters, etc.) are entered in the initial section of the program. These input parameters fall into main categories: geometric parameters (stroke, bore, connecting-rod length, crank radius, and compression ratio) and thermodynamic parameters (maximum combustion pressure, initial temperature, and heat release rate). Grouping these data into a single configuration file ensures the complete reproducibility of the calculations. The specifications of the investigated six-cylinder in line, four-stroke diesel engine (model MIDR 0635 40 M/3) are summarized in Table 1.

Table.1. Engine characteristics

| Engine characteristic | Value |
|---|---|
| Total displacement[liter] | 12.02 |
| Stroke [mm] | 140 |
| Diameter [mm] | 135 |
| Compression ratio | 18/1 |
| Mean piston speed [m/s] | 9.33 |
| Maximal power [kW] | 235 |
| Maximal Torque [N.m] | 1450 |
| Mass of piston [kg] | 3 |
| Mass of connecting rod [kg] | 5.15 |
| Mass of rings [kg] | 0.125 |
| Mass of piston pin [kg] | 1.73 |
| Connecting rod length[mm] | 265 |
| Crankpin diameter [mm] | 84 |
| Crankpin length[mm] | 55 |

The calculation procedure unfolds in two successive and interdependent steps. The first step treats the problem from a purely kinematic point of view: for each crank angle, the position, velocity and acceleration profiles of the crankshaft are calculated by computer simulation, if the engine operates at constant angular speed — a classic hypothesis under steady-state conditions, justified by the smoothing effect of the flywheel. The second step involves feeding these kinematic profiles into the dynamic module of the algorithm to calculate the forces applied to the crankpin: the tangential force (T) generating the engine torque, the normal force (Z) exerted on the bearings, the side thrust force (N) on the cylinder wall, and the total resultant load (Q) on the crankpin. These forces are calculated successively for the two connecting rod models, enabling a term-by-term comparison at each angular step of the engine cycle and at different operating speeds (1400 to 2200 rpm).

The algorithm for computing the dynamic forces applied to the slider-crank system was developed and implemented using FORTRAN Power Station 4.0 (Microsoft Developer Studio). The code is structured into two main modules: a kinematic module computing the position, velocity, and acceleration profiles of the crankshaft for each crank angle, and a dynamic module computing the forces applied to the crankpin (N, T, Z, Q) for both connecting-rod models, using the cylinder pressure data obtained from the thermodynamic-cycle computation. It should be noted that the governing equations of the effective model are significantly more complex than those of the standard simplified model: they simultaneously integrate the longitudinal and rotational inertial contributions of the actual connecting rod, representing a major advantage of the proposed methodology over current industrial approaches, particularly at high speeds where inertia forces become dominant [10].

## 3 Results and discussion

### 3.1 Results of dynamic analysis

#### 3.1.1 Crankpin loads analysis

The magnitude and direction of the forces acting on the connecting-rod big-end bearing can be calculated as a function of crank angle (CA) using the equations provided above. The resulting bearing load is typically illustrated using polar diagrams (Fig. 2). These diagrams provide a comprehensive visual tool for simultaneously analyzing the load distribution over the entire engine cycle. Three essential pieces of information are directly extracted from them: the amplitude of the maximum load, which is necessary for the sizing and lubrication of the bearings; the maximum inertial load, which is crucial for sizing of the connecting-rod cap and its bolted joint; and finally the location of the minimum load, which dictates the choice of the parting plane between the connecting rod and its cap [30].

Analyzing the polar diagrams (Fig. 2) reveals two major loading events during the engine cycle. The first corresponds to the combustion peak, where the resultant force is nearly centered along the connecting rod axis, just after 0° CA (with TDC chosen as the angular origin). This peak results from the maximum combustion pressure, acting perpendicularly to the crankpin and constitutes the most intense loading of the cycle. The second peak occurs at TDC during valve overlap (360° CA); here, the cylinder pressure is low, but the inertia forces resulting from the deceleration of the piston assembly create a secondary load concentrated on the connecting-rod cap. For the heavy-duty diesel engine investigated (MIDR 0635 40 M/3), cylinder pressures are highly elevated. Because the rotational speed is relatively low, the inertial component remains significantly weaker than the gas pressure component, which is reflected in the characteristic elongated shape of the polar diagrams obtained.

The polar diagrams in Figure 2 are plotted in a coordinate system fixed to the connecting rod five engine speeds: 1400, 1600, 1800, 2000 and 2200 rpm. At low speeds, inertial effects on the load are minimal — as evidenced by the olive-shaped area on the left side of the diagram — and the load is heavily dominated by gas pressure. As the speed increases, the inertial component grows with the square of the engine speed, causing a progressive widening of the diagram. Quantitatively, the tensile load on the connecting rod at TDC at the end of the exhaust stroke (0° CA) reaches 30 to 45 kN, a value higher than the maximum compressive load of 25 kN at 540° CA. At 180° CA (BDC, end of intake), the compressive load results exclusively from inertial effects, since the cylinder pressure is practically zero at this instant. Comparing the two models, the simplified version tends to overestimate the inertial force component. Additionally, the application point of the load on the crankpin shifts significantly compared to the effective model due to centrifugal forces. These deviations confirm that the simplified model introduces non-negligible errors in the rotational inertial torques, as anticipated by the work of Shiao and Moskwa [10].

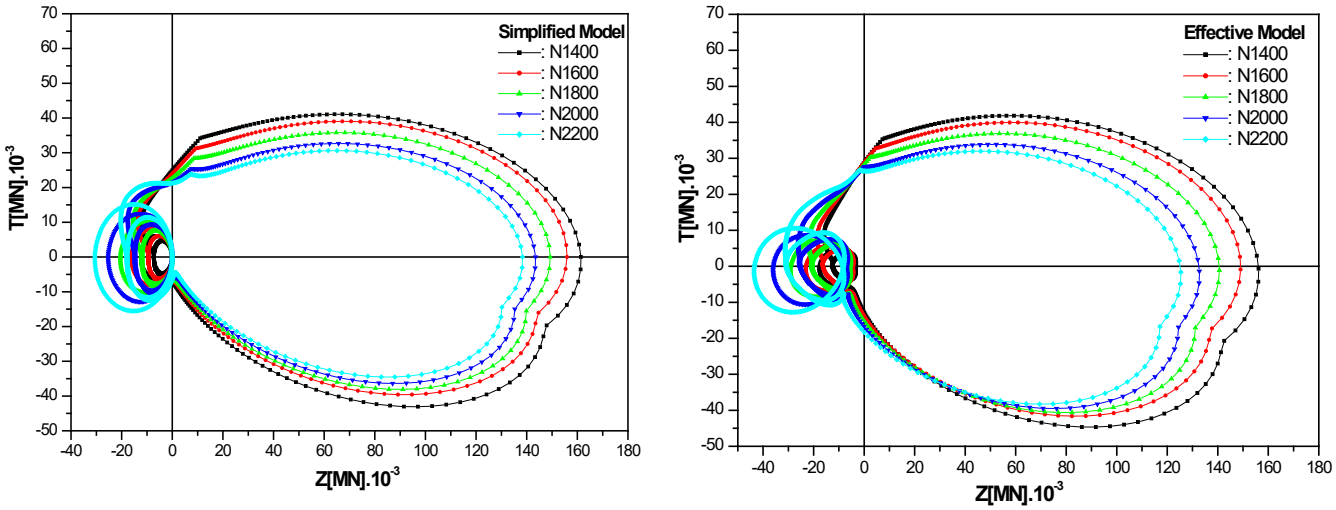


Fig. 2. Polar diagrams load (Q) on the crankpin

The lateral load component (N), which represents the piston thrust against the cylinder wall, exhibits a behavior that clearly highlights the deviations between the two models (Fig. 3). At high engine speeds, this component displays a relatively low peak value (approximately 10 kN). This behaviour is explained by the transition between two dominant loading regimes: at low speeds, the amplitude of (N) is primarily governed by the indicated torque effect (gas pressure); as speed increases, inertia forces become dominant and tend to partially counterbalance the pressure forces. The deviations between the two models are most pronounced for this component, confirming that the lateral load is the most sensitive indicator of the moment of inertia error (Jf) inherent in the simplified model.

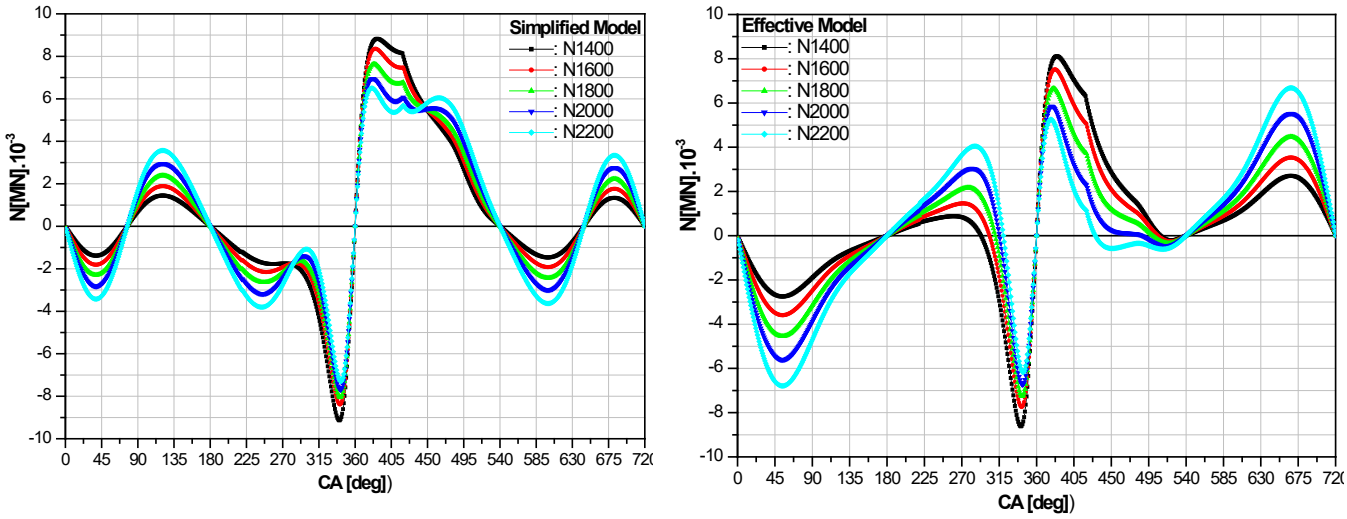


Fig. 3. Load component (N)-Piston action on the cylinder wall

The tangential load component (T), which generates the engine torque, is presented in Figure 4. During the intake stroke, its magnitude remains low (approximately 15 kN). During the compression stroke, (T) grows in the negative direction to approximately −50 kN, then rises sharply to reach a maximum positive peak of 50 kN at the onset of combustion. This peak value is consistent with the maximum combustion force $P_{max}$ = 187.55·10⁻³ MN used in the analysis. Following combustion, (T) decreases steadily until it drops to zero at the beginning of the exhaust stroke. This cyclic profile is identical for both connecting-rod models, confirming that the tangential load is primarily governed by the thermodynamic cycle and is largely insensitive to the moment of inertia error.

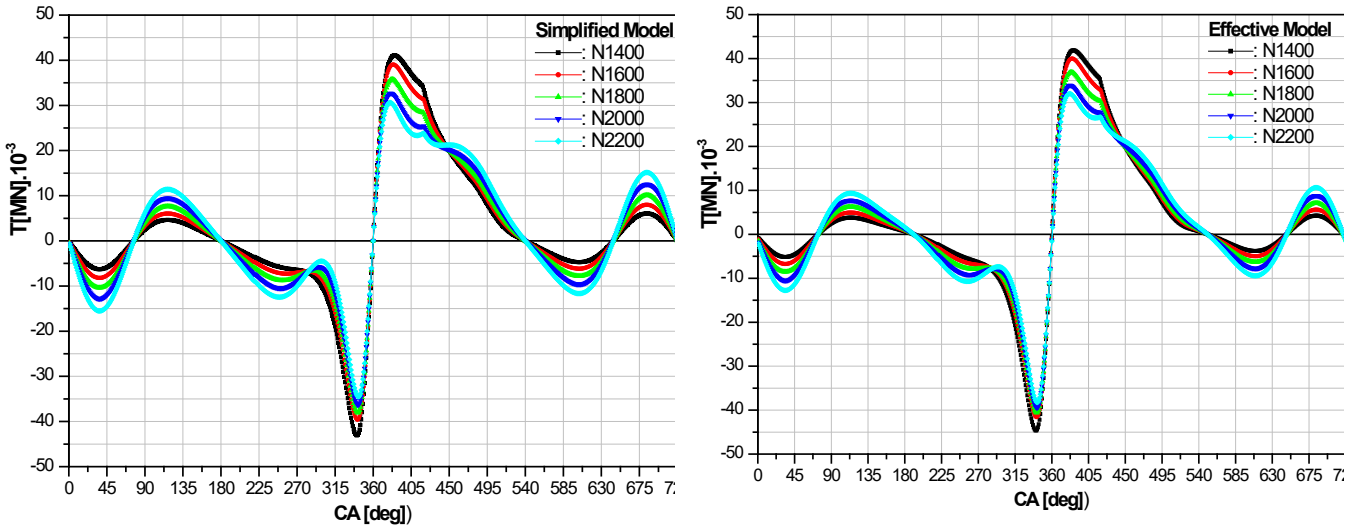


Fig. 4. Tangential load on crankshaft radius (T)

The radial load component (Z), applied to the connecting rod big end in the direction of the crankshaft radius, is presented in Figure 5. Its amplitude is comparable to that of the total load (Q). This force is negative for most of the cycle (opposite to the direction of piston movement), except during combustion when it reaches its maximum positive value. As an internal force, it represents a reaction to external forces such as pressure and inertia forces. During combustion, the results of the two models are comparable, however, outside this phase, the simplified model significantly underestimates this load, with cancellations at points corresponding to 67.5° CA. With the effective model, the profile remains quasi-regular around an average value, reflecting a physically more faithful representation of reality.

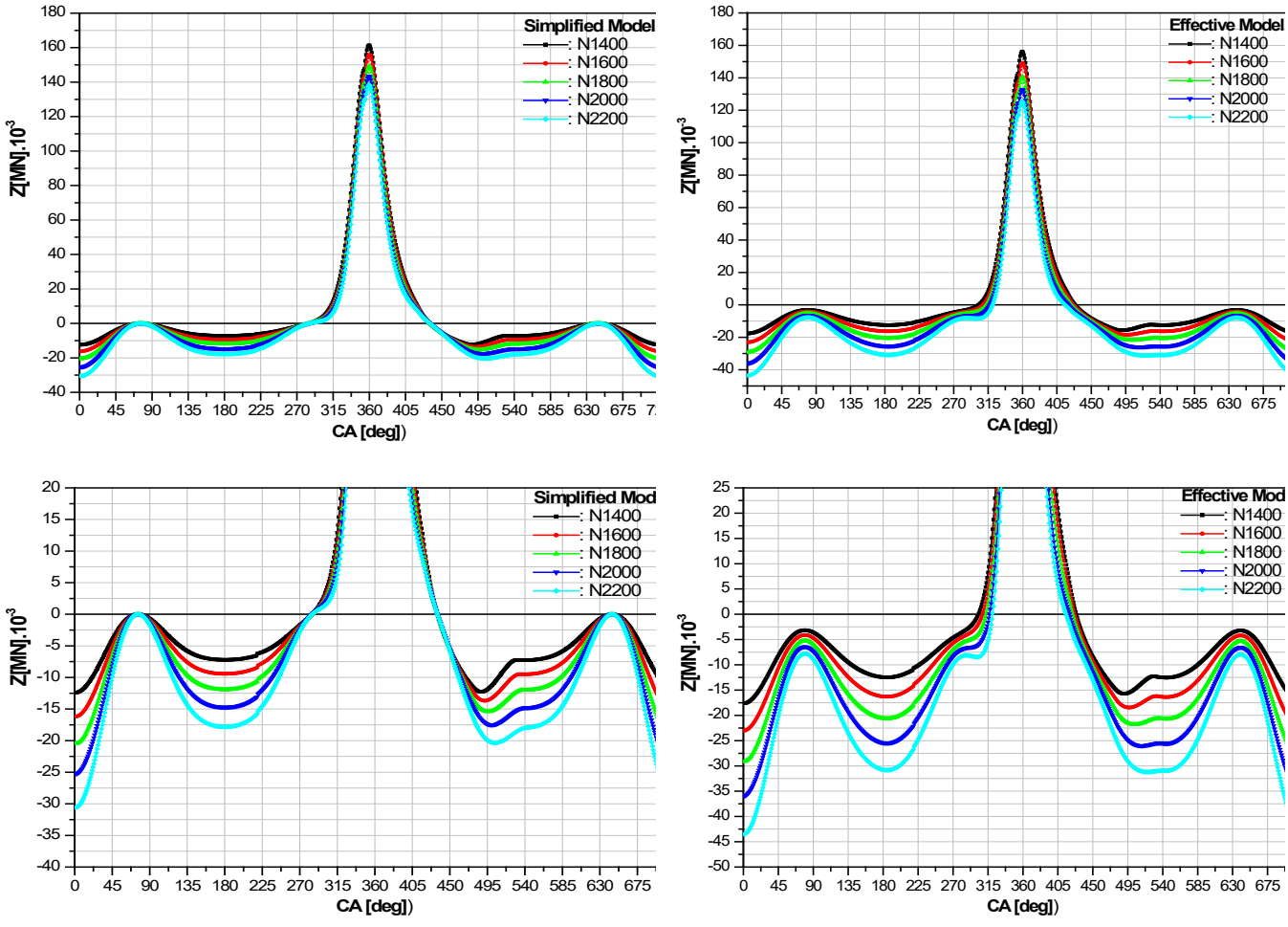


Fig. 5. Radial load along crankshaft radius (Z)

The total resultant load (Q) applied to the crankpin, calculated at 1200 rpm (maximum torque) and 2000 rpm (maximum power) for both models, is presented in Figure 6. At low speed, a very high thrust on the connecting rod, exceeding 160 kN, is observed over a short period at the end of the compression stroke and at the beginning of the expansion stroke. This thrust results from the quasi-impulsive pressure rise during combustion — typically over 10 to 20° crank angles for a direct injection diesel engine — whose dynamic component cannot be instantaneously absorbed by the lubricant film, thus generating the shock phenomenon on the crankpin bearing. As speed increases and inertia forces progressively grow, a balance between gas forces and inertia forces can be established, allowing the shock phenomenon to disappear.

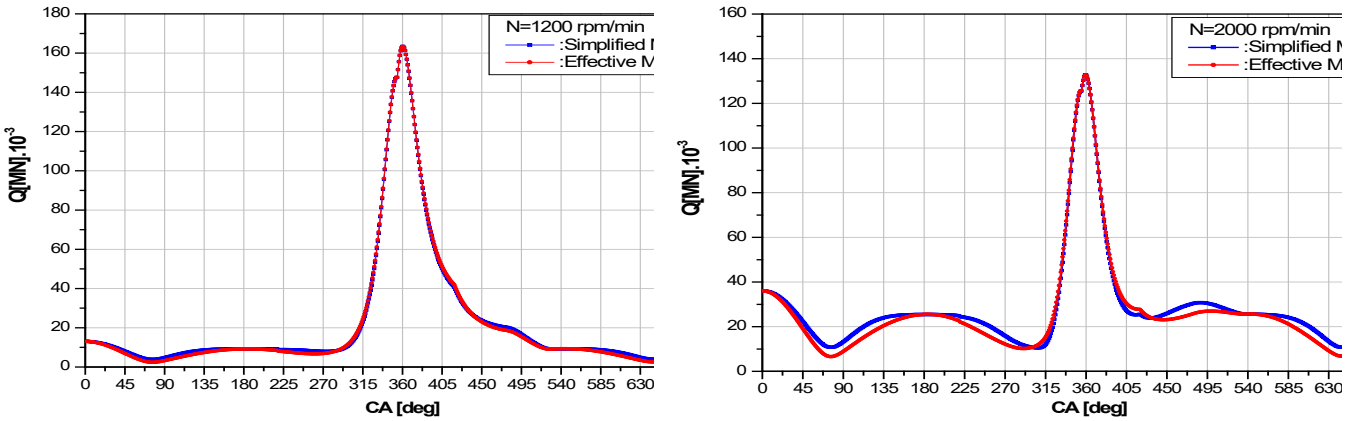


Fig. 6. Total load (Q) applied on the connecting rod big-end and crankshaft-pin linkage

Reciprocating mechanisms have a variable inertia due to the change in geometry relative to the crankshaft axis of rotation. Figure 7 illustrates the evolution of these variable inertia terms over an engine cycle. These components follow a periodic and regular profile, well represented by a sinusoidal function that repeats identically at each crankshaft revolution [30]. The stroke-by-stroke analysis confirms the expected physical trends: during the intake stroke, inertia forces remain low; as top dead center (TDC) is approached at the end of compression stroke, they increase significantly; at the moment of auto-ignition, the sudden release of energy amplifies the gas pressure forces (inertia forces), which reach their maximum values; finally, during the exhaust stroke, these forces gradually decrease, contributing to the reduction of loads on the crankshaft at the end of the cycle.

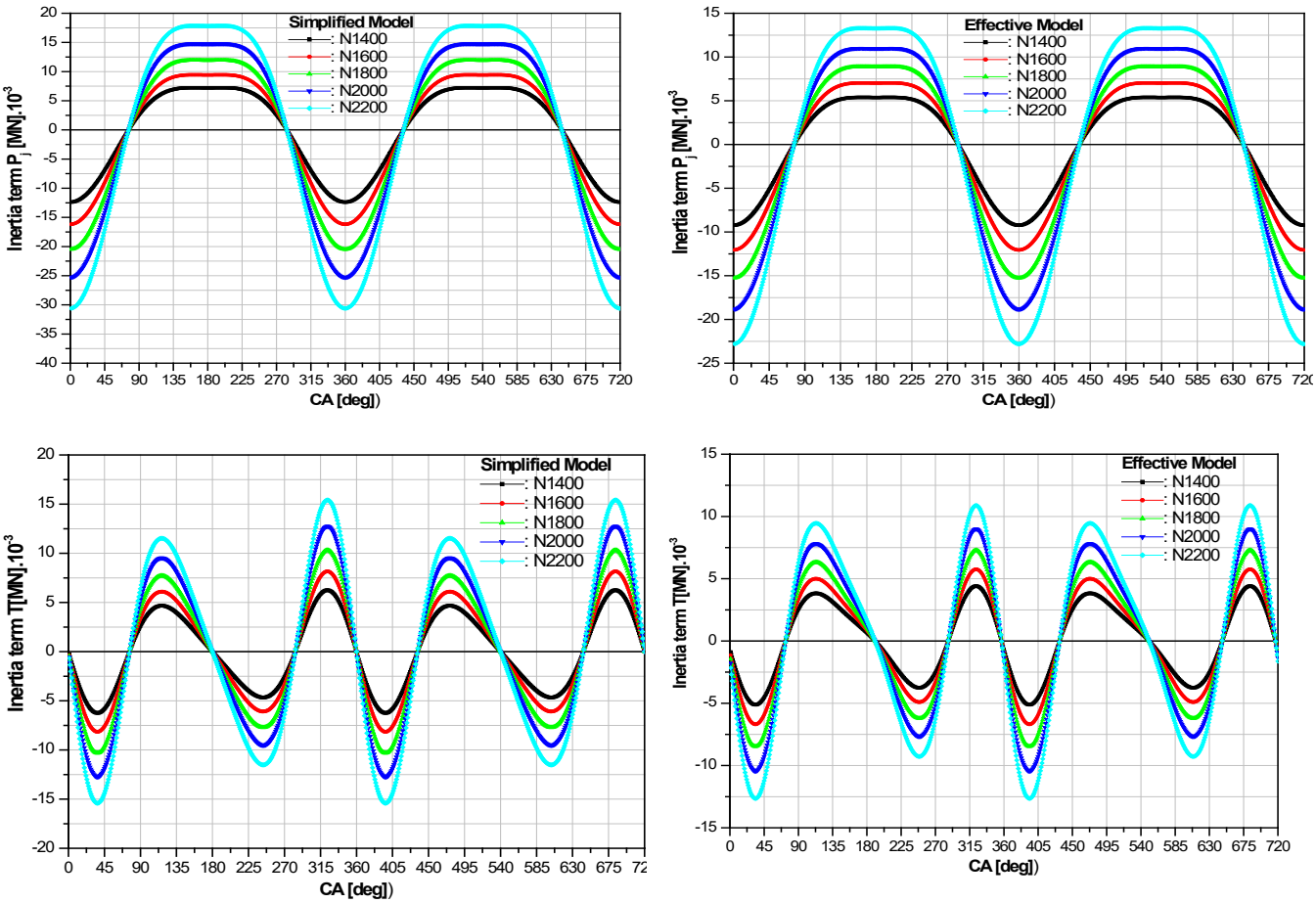

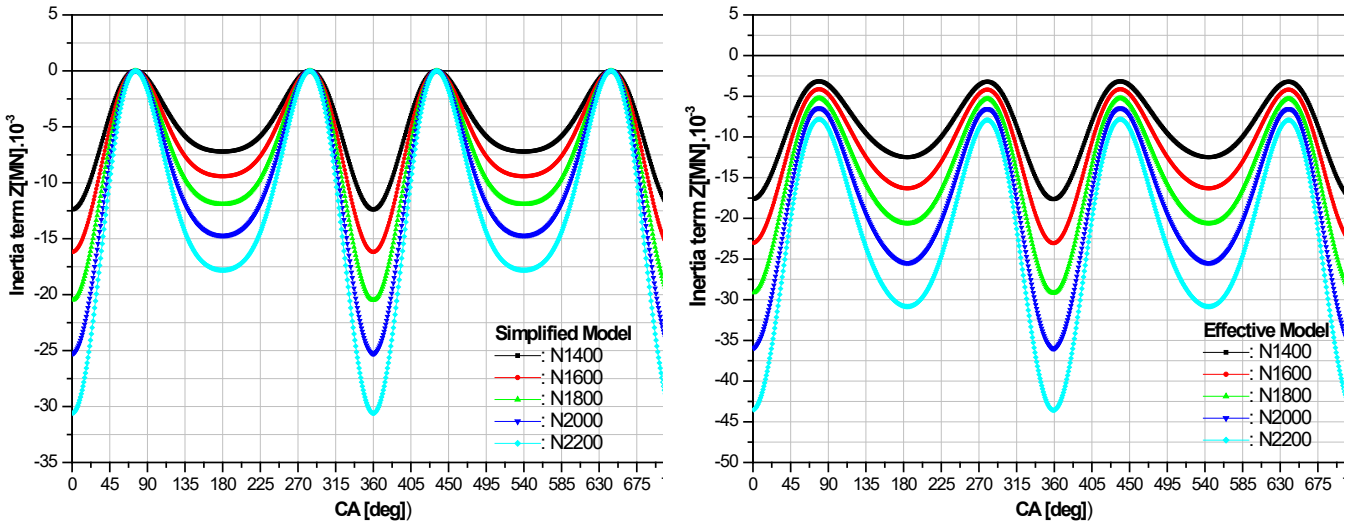


Fig. 7: Inertia terms of loads T, Z (from Q) and Pj(from P∑)

Generally, during the intake stroke, inertia forces remain relatively low as the piston moves in a direction that does not cause sudden changes in crankshaft motion. As the piston moves upwards to compress fresh air in the combustion chamber, inertia forces begin to increase (fluctuate additionally). As the piston approaches TDC, inertia forces reach a maximum peak, since the piston undergoes its highest deceleration before changing direction.

When combustion of the air-fuel mixture occurs, inertia forces can be significantly influenced; a major peak is recorded during combustion. At the moment of auto-ignition in the combustion chamber, there is often a distinct peak in inertial forces. This is due to the sudden release of energy and pressure generation, which affects piston movement. Inertial forces during this phase can exert maximum load on the crankshaft and support bearings, requiring a robust design to absorb these stresses. As the piston begins to move upwards to evacuate burnt gases, inertia forces change once again. After combustion, inertia forces generally decrease as the piston moves in the opposite direction, facilitating the release of burnt gases. Inertia forces decrease as the piston descends or moves towards the BDC, contributing to a reduction in crankshaft loads.

### *3.1.2 Characteristics of crankpin bearing working conditions*

The characteristic of the crankpin bearing working condition is given by the parameter: $\lambda_{cr} = v \cdot N/kmax$, where $k_{max} = Q_{max}/(l_p \cdot d_p)$, where: v represents the dynamic viscosity of the oil [cP]; N is the engine speed [rpm]; $Q_{max}$ is the maximum load [N]; $l_p$ is the crankpin length [m]; $d_p$ is the crankpin diameter [m]. The specific load for diesel engines and big-end bearings is [80–160] kg/cm². The maximum specific load can reach 800 kg/cm². The tolerance range of the characteristic parameter ($\lambda_{cr}$) is [100–250] cP·rpm/kg·cm$^{-2}$. From Figure 8, the values obtained for the specific loads ($k_{max}$) and the characteristic parameter ($\lambda_{cr}$) remain within the standard characteristics of the bearing working conditions. These results confirm that the MIDR 0635 40 M/3 engine operates in an acceptable lubrication regime for both connecting rod models.

The shock parameter ($\chi$) is defined by the ratio $\chi = k_{max}/k_{mea}$, where $k_{mea}$ is the average specific load over the engine cycle. This parameter quantifies the intensity of the dynamic impact suffered by the crankpin bearing during the abrupt passage from inertia load to combustion load in the vicinity of TDC. From a physical point of view, the shock phenomenon is directly governed by the pressure rise rate (dp/dθ, in MPa/°CA) in the combustion chamber: at auto-ignition, the cylinder pressure rises quasi-impulsively over an interval of only 10 to 20° CA, generating a rapid variation of the resultant force on the crankpin that the lubricant film cannot instantaneously absorb. When ($\chi$) exceeds the standard limit value ($\chi \leq 4$) for in-line diesel engines, the hydrodynamic film risks local rupture, leading to transient metal-to-metal contact. In the present study, the values obtained are $\chi$=4.642 with the simplified model and $\chi$=4.950 with the effective model. These values are slightly above the admissible limit, with a 6.6% deviation between the two models, signaling an increased risk of shock at low speeds where combustion is dominant.

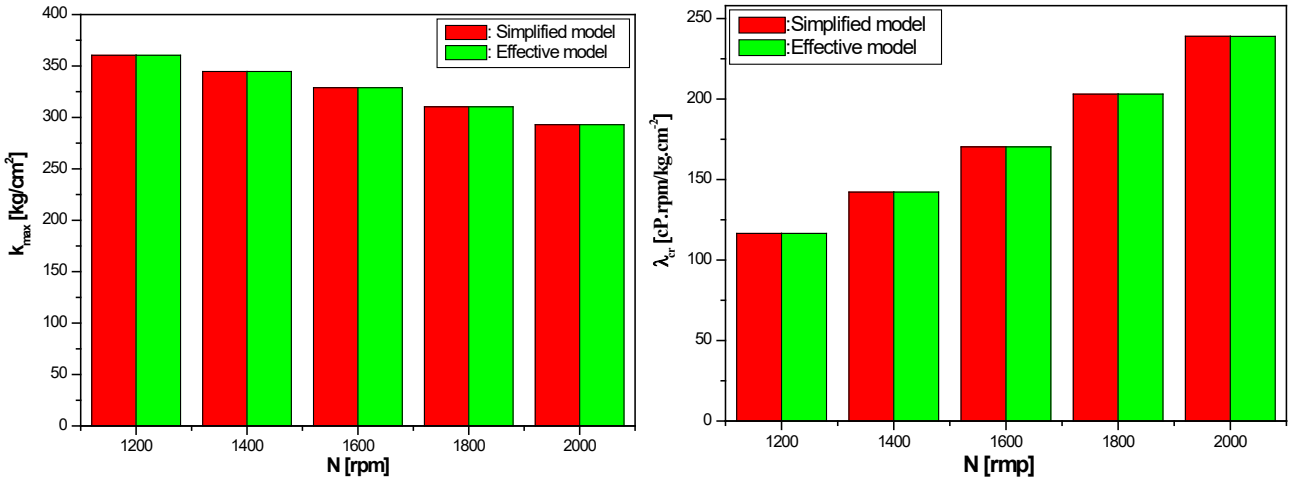


Fig. 8. Characteristics parameters of crankpin bearing working conditions

In principle, to limit the shock, it is necessary to increase the value of the centrifugal inertia forces ($p_{k0}$) and, consequently, the value of the connecting rod mass involved in the rotational movement ($m_{cbe}$). However, this recommendation must be considered with caution in the current context of thermal engine development: the global downsizing trend aims precisely at reducing moving masses in order to decrease inertia losses and $CO_2$ emissions. An increase in $m_{cbe}$ would counter to this objective by increasing unbalanced centrifugal forces — generating additional efforts on the main bearings, disturbing the dynamic balancing of the crankshaft, and increasing the moment of inertia of the system to the detriment of the engine transient response. Rather than a direct modification of masses, two technically coherent alternatives are recommended: on the one hand, geometric optimization of the crankpin/web fillet — increasing the fillet radius and introducing compressive residual stresses by shot preening — to reduce stress concentrations without modifying the system mass; on the other hand, tribological optimization of the bearing — adjusting the lubricant viscosity and operating clearance — to improve the capacity of the hydrodynamic film to absorb shocks.

Generally, a shock occurs when the force impulse and, consequently, the momentum and velocity of a solid change from one finite value to another in an extremely short time. The accelerations during impact reach very high values. Since the duration of the impact is negligible, the displacements of the solid points during this same time are also negligible. Two practical conclusions can be formulated [31]: the actions of forces during the impact are negligible, and the displacements are also negligible. In the context of the crankpin bearing, it is therefore the physical nature of the contact — material stiffness, fillet geometry, lubricant film properties — that determines the capacity of the bearing to absorb the shock impulse without damage, justifying the particular attention paid to the geometric and tribological optimization of the crankpin in the present study.

### *3.2 Numerical analysis*

The crankpin is subjected to high stress, particularly at the crankpin/web intersection. Due to these high dynamic loads, two types of stress occur at the crankpin: bending and torsion. Bending causes compressive and tensile stress, while torsion causes shear stress. The crankpin is also subjected to loads that cause shock and material fatigue. In the framework of the present study, a numerical simulation is carried out on the crankpin of a multi-cylinder diesel engine using Abaqus software. This analysis pursues three complementary objectives: to identify the critical sections of the crankpin, to quantify the variation of bending and torsional stresses according to two loading hypotheses, and to evaluate the mechanical strength of the component by means of the Von Mises criterion. The simulation data are established on the basis of the engine data sheet supplied by the manufacturer, a detailed thermodynamic study of the engine cycle, and the results of the previously conducted dynamic analysis.

The crankshaft material is 42C4 steel (quenched and tempered), in accordance with the technical specifications provided by the manufacturer (Berliet/Renault Trucks). The mechanical properties retained are Young's Modulus of 210 GPa, Poisson's ratio of 0.3, Modulus of rigidity of 80 GPa, and a density of 7850 kg/m3. The yield limit retained is σy = 560 MPa. This value corresponds to the original specification of the studied engine and constitutes a conservative assumption, considering the effects of operating temperature and uncertainties regarding the mechanical properties in service. It should be noted that this value influences only the safety factor calculation, without modifying the calculated stress distribution or the validity of the comparison between the analytical and numerical approaches. All analyses conducted are based on the linear elastic properties of the crankshaft material. In order to guarantee the independence of the results with respect to mesh density, a systematic convergence study was carried out prior to the final analysis. Four refinement levels were tested at the crankpin/web fillet junction and contact zones.

The safety factor is defined by $N = \sigma_y/\sigma_{VM}$, where ($1.3 \leq N \leq 5$). The Von Mises stress theory ($\sigma_y/\sigma'$) is useful for calculating the safety factor to prevent failure. It should be noted, however, that this safety factor constitutes a static indicator allowing the verification of the absence of plastic deformation (plasticization) under maximum loading, but

cannot substitute for a complete fatigue analysis. Due to the cyclic and multiaxial nature of the applied loads — a combination of bending and torsion at variable amplitude during the engine cycle — a complete durability analysis must rely on an adapted multiaxial fatigue criterion, such as the Dang Van criterion, the Crossland criterion, or the Haigh diagram, which constitute a direct and high-priority perspective of the present study.

Two loading hypotheses are used to evaluate material strength. The first hypothesis assumes that the critical position is located at top dead centre at engine ignition (TDC); hence, the maximum effort due to gas pressure is used as the source load ($P_{max}$ = 187.55·10⁻³ MN). The load applied to the crankpin journal in the finite element model is represented by an equivalent uniformly distributed pressure acting over a 60° load zone, corresponding to the loaded region of the bearing. Regarding boundary conditions, the main crankshaft bearing is modeled as a fixed support (clamped boundary condition) by setting both translational and rotational degrees of freedom to zero. The integration of a coupled elasto-hydrodynamic (EHD) lubrication model, as proposed by Yin et al. [21], is identified as a direct perspective of this work.

Bending stresses, shear stresses, and Von Mises stresses are shown in Figure 9. The crankpin undergoes bending, which gives a maximum stress in its middle: analytical computation gives $\sigma_b$ = 140.20 MPa and numerical computation gives $S_{11}$ = 138.8 MPa (see Fig. 9-a), representing a deviation of less than 1%. For shear stresses, analytical computation gives $\tau_{2sh}$ = 22.56 MPa and numerical computation gives $S_{12}$ = 18.77 MPa (see Fig. 9-b). The global comparison stresses (Von Mises stresses) are analytical computation $\sigma_2$ = 140.20 MPa and numerical computation S = 128.9 MPa (see Fig. 9-c), indicating a deviation of 8%. The yield stress for the crankpin is $\sigma_y$ = 560 MPa. The numerical Von Mises stresses represent 23% of the yield limit, corresponding to a safety factor N = 4.34, which is within the admissible range (1.3 ≤ N ≤ 5). The Von Mises stress map confirms that the maximum value is reached at the crankpin/web fillet junction, identifying this zone as the critical site for fatigue crack initiation, in agreement with the observations in the literature [4, 11].

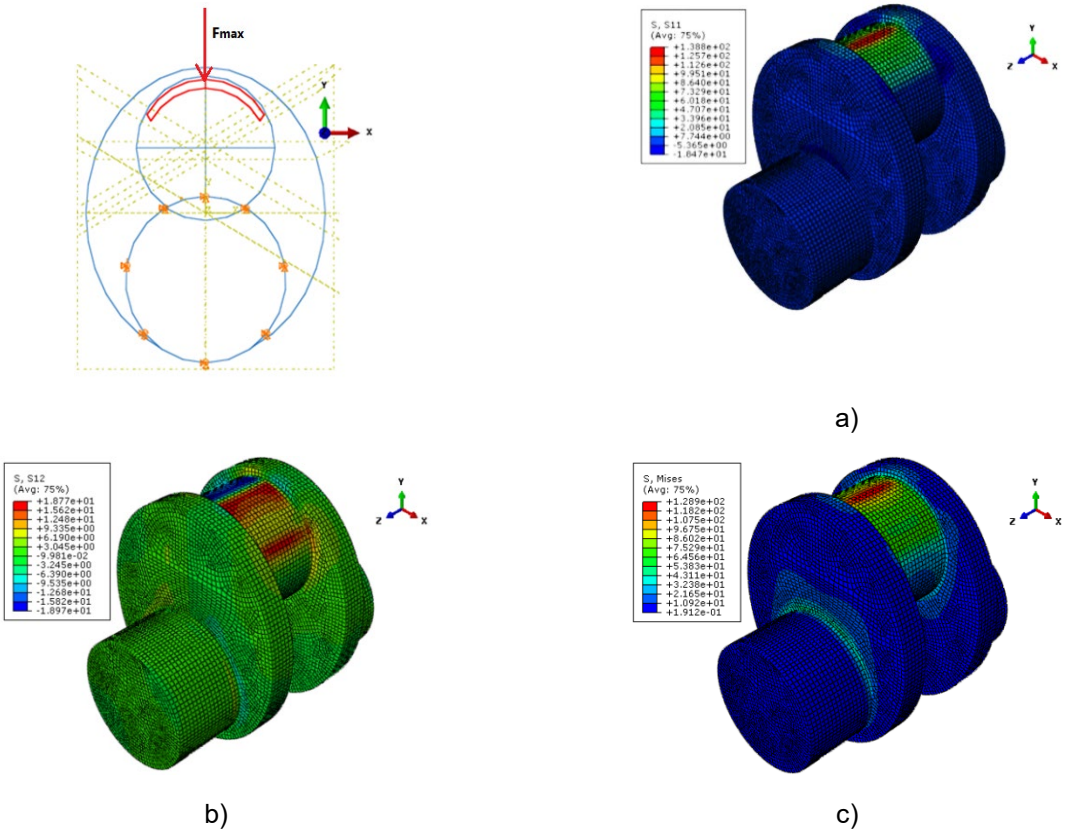


Fig. 9: Stresses state and boundary conditions using the 1st hypothesis (TDC): a) bending stresses b) shear stresses c) Von-Mises stresses

The maximum load occurs at TDC, where the combustion process takes place; at this moment, the acting force on the crankshaft is just a bending load. The peak bending load decreases as the engine speed increases because of the load sources. The force caused by combustion is nearly constant at the different engine speeds since the same maximum pressure is used for all engine speeds. However, the load caused by inertia increases in magnitude as the engine speed increases. A comparison of the different stresses using the first hypothesis is presented in Fig.10.

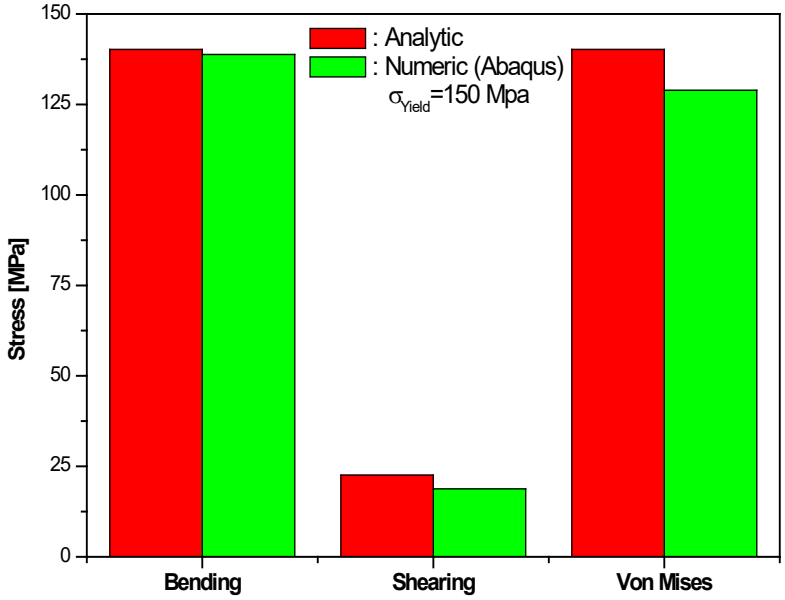


Fig. 10. Comparison of different stresses (1st hypothesis)

The second hypothesis, suppose that the critical position is caused by the maximal tangential effort, hence, the load applied by the connecting rod (Fcr= 163.63.10-3 MN) on the crankpin is subdivided into two components: tangential load, T=54.93.10-3 MN, and normal load, Z=N=161.68.10-3 MN (see Fig.11). In this case, each crankpin undergoes a bending which gives rise to a maximum stress in its middle, and where analytical computation gives σb=122.32 MPa and numerical computation gives S11=121.2 MPa (see Fig.11-a). A shear stress S12 acting in the y direction on the face normal to the x direction, where analytical computation gives τ2sh=19.68 MPa and numerical computation gives S12=16.38 MPa (see Fig.11-b). A twist that will cause maximum stress on the periphery, where analytical computation gives τ1sh=16.52 MPa and numerical computation gives S12=16.38 MPa (see Fig.14-b). The global stress of comparison stresses an:alytical computation gives σ1=125.62 MPa, and numerical computation gives S=112.5 MPa (see Fig.11-c). The yield stresses for cranthe the thenk-pin-to-pinning hypothesis are : σy The safety factor using these values can range from 4.46 to 4.97, which verifies the safety condition.

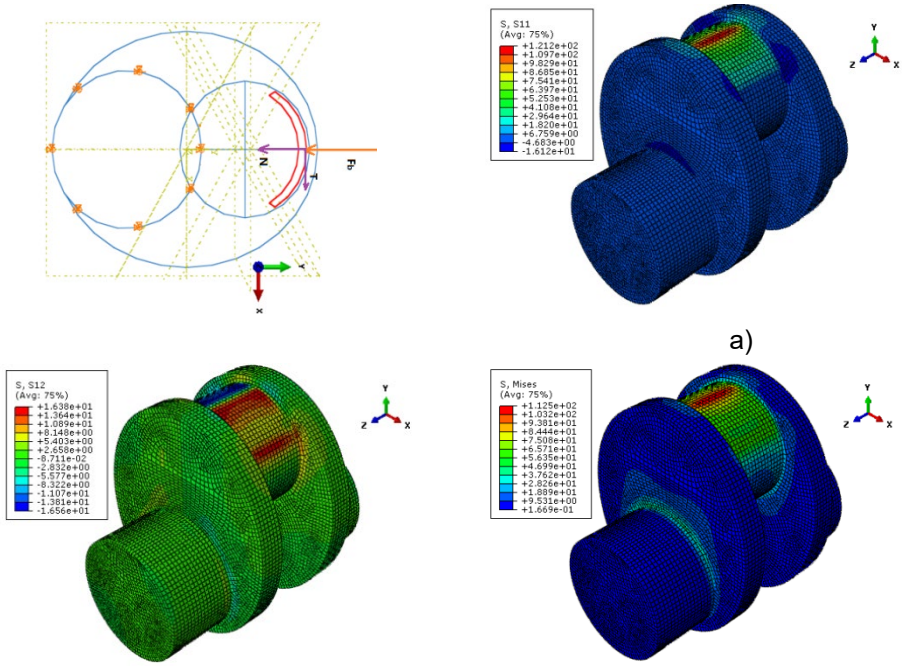


Fig. 11. Stresses state and boundary conditions using the 2nd hypothesis: a) bending stresses b) shear stresses c) Von-Mises stresses

Comparison of the different stresses using the second hypothesis is indicated in Fig.12. Regarding the twist loads, they have no effect on the range of Von Mises stresses at critical locations; they are located on the bearings of the crankpin. The bending and torsional loads occur at different times and locations. In addition, at the peak of the bending load, the magnitude of the torsion load vanishes. In accordance with the literature data [32], the torsion load

represents less than 7% of the bending load, which justifies the priority given to bending resistance in the sizing of the crankpin.

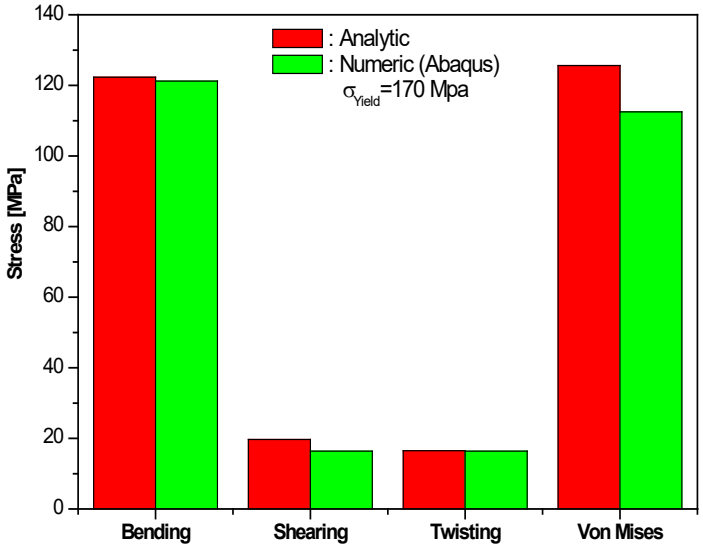


Fig. 12. Comparison of different stresses (2nd hypothesis)

The crankpin bending and twist deformations are illustrated in Fig.13. The safety factor to prevent failure using the two hypotheses is also presented in Fig.14.

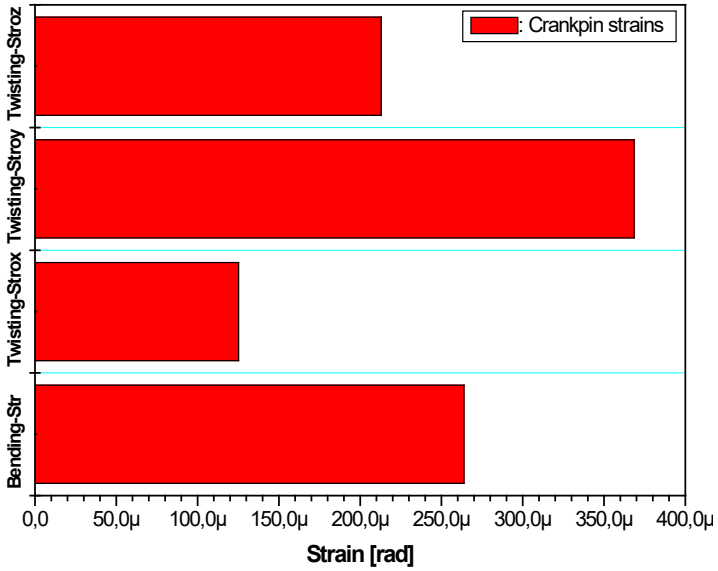


Fig. 13. Crankpin bending and twist deformations

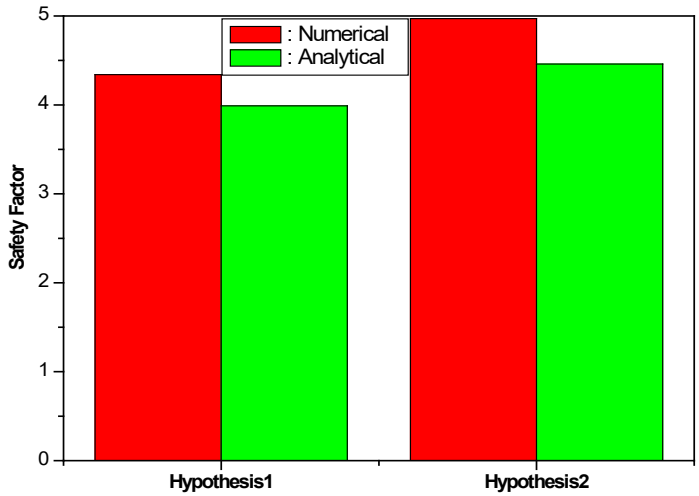


Fig. 14. Safety factor of crankpin material

To investigate shear stresses and strain distributions under critical loading conditions, using Abacus software, an applied pressure of over 120° at four locations on the crankpin bearing was prescribed. These locations are labeled as a, b, c, and d (see Fig.15). From the load polar diagram of the crankpin, loads applied at locations (a, b, c, and d) are (27.90 MPa, 13.23 MPa, 23.97 MPa, and 4.34 MPa), respectively. From the stress state (see Fig. 16), it appears that the lower face of the crankpin corresponding to the exhaust stroke is the most stressed and deformed part ($S_{12}$ = 34.10 MPa, $E_{12} = 4.43 \cdot 10^{-10}$, Fig. 16-c), followed by the side face corresponding to the expansion stroke ($S_{12}$ = 24.34 MPa, Fig. 16-b), then the upper face corresponding to the compression stroke ($S_{12}$ = 13.56 MPa, Fig. 16-a), and finally the side face corresponding to the inlet stroke which is the least stressed and deformed ($S_{12}$ = 4.91 MPa, $E_{12} = 6.38 \cdot 10^{-11}$, Fig. 16-d). This ranking faithfully reflects the hierarchy of loads from the polar diagram and confirms the physical consistency of the numerical model.

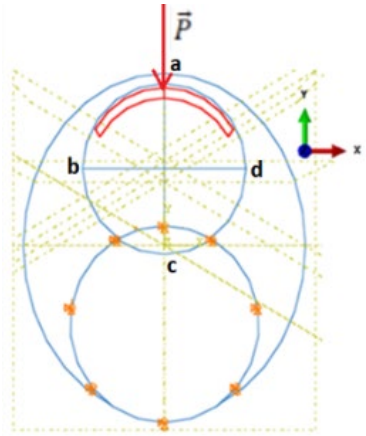


Fig. 15. Locations on the crankpin where the shear stress and strain variations were calculated over one engine cycle

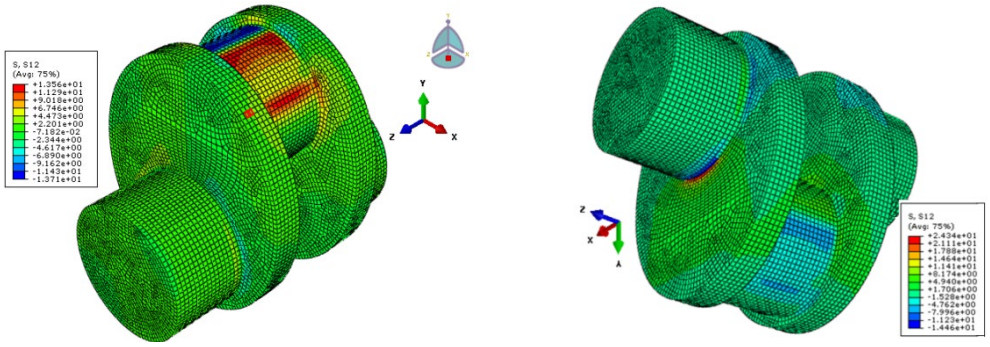

a) b)

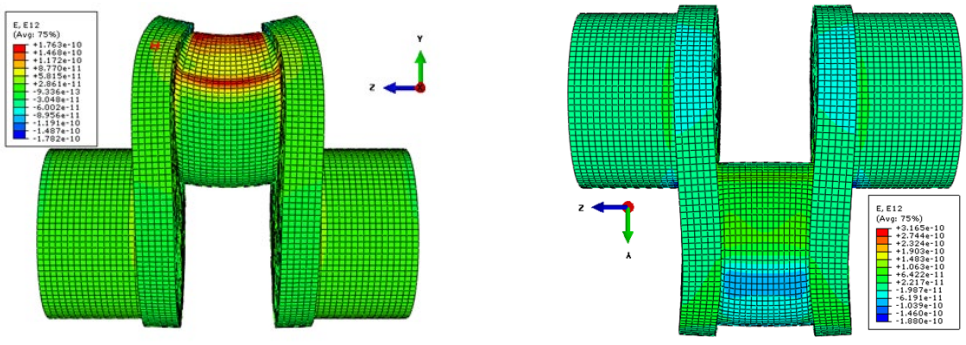

c) d)

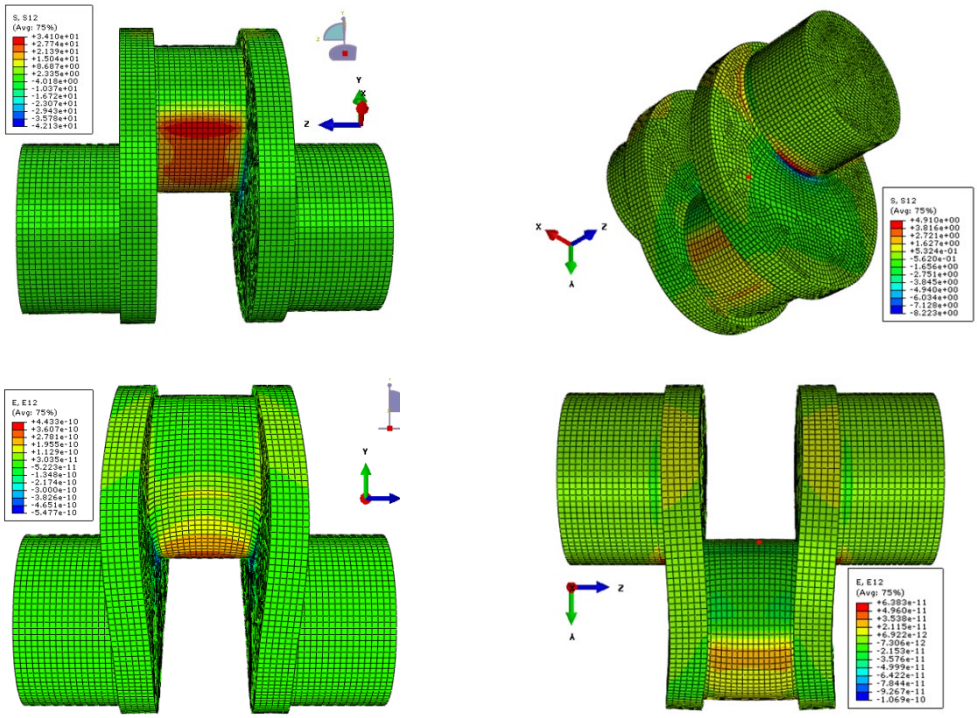

Fig. 16. Shear stresses and shear strains distribution under critical loading condition

## 4 Conclusions

The present study has made it possible to analyze the dynamic behaviour of the crankshaft-connecting rod system of a six-cylinder in-line diesel engine (MIDR 0635 40 M/3) and to evaluate the loads applied to the crankpin as well as the mechanical stresses developed within it. The results show that the difference between the two connecting rod models is most perceptible on the piston lateral load component (N). The simplified model systematically overestimates the inertia forces, with deviations reaching 6.6% on the shock parameter compared to the effective model, due to the moment of inertia error (Jf ≠ 0) inherent to the two-lumped mass model. In modern high-speed machines, the balance of inertia forces constitutes a persistent concern for the designer.

The values obtained for the shock parameter are 4.642 with the simplified model and 4.950 with the effective model, both slightly above the standard admissible limit ($\chi \leq 4$) for in-line diesel engines. It is therefore recommended to increase the big-end connecting rod mass (mcbe) in order to increase the centrifugal forces ($p_{k0}$) and thus reduce the maximum specific load ($k_{max}$). However, this recommendation must be nuanced in view of the global downsizing trend: rather than a direct increase in $m_{cbe}$, geometric optimization of the fillet (fillet radius + shot peening) and tribological optimization of the bearing constitute alternatives more coherent with modern design requirements.

According to the results of the finite element numerical analysis, the Von Mises stress values are lower than the material yield stresses. The maximum analytical stress is 140.20 MPa, and the corresponding numerical value is 128.9 MPa, a deviation of less than 10%, confirming the coherence and reliability of the approach. The safety factor is within the admissible range ($1.3 \leq N \leq 5$), which a posteriori justifies the hypothesis of linear elastic behaviour. The lower face of the crankpin, corresponding to the exhaust stroke, is the most stressed part ($S_{12}$ = 34.10 MPa). The torsion load represents less than 7% of the bending load. The maximum cyclic load produced on the crankpin corresponds to that resulting when the piston is at top dead centre just after combustion.

The calculation results are compared with those obtained analytically, and the reliable stresses thus obtained are used as critical data in the fatigue analysis and in the crankpin and crankshaft optimization process in general. In perspective, a multiaxial fatigue analysis (Dang Van criterion or Haigh diagram), the integration of a coupled elasto-hydrodynamic lubrication model, and the consideration of transient regime constitute the natural extensions of this work to improve the accuracy of the evaluation of the crankpin's actual operating conditions.

## 5 Acknowledgements

This work has been carried out at LMA Laboratory, University of Sciences and Technology Mohamed Boudiaf of Oran (USTMBO)-Algeria. We would like to thank the laboratory director for his interest in this work and for the assistance he provided us.

## 6 References

[1] Kumar, R., Gupta, T., & Bajaj, R. (2015). Conventional design and static stress analysis of IC engine component (crank pin) using the finite element method. *Advances in Automobile Engineering, 4*(1). https://doi.org/10.4172/2167-7670.1000118

[2] Mrdja, P. D., Miljic, N., Popovic, S. J., & Kitanovic, M. A. (2018). Method for quick estimation of engine moment of inertia based on an experimental analysis of transient working process. *Thermal Science, 22*(3), 1215–1225. https://doi.org/10.2298/TSCI170915224M

[3] Zweiri, Y. H., Whidborne, J. F., & Seneviratne, L. D. (2001). Detailed analytical model of a single-cylinder diesel engine in the crank angle domain. *Proceedings of the Institution of Mechanical Engineers, Part D: Journal of Automobile Engineering, 215*(11), 1197–1216. https://doi.org/10.1243/0954407011528734

[4] Parejiya, B. N., Morabiya, D. B., & Amit, S. (2014). Design and optimization of crankpin: A review. *International Journal for Research in Applied Science and Engineering Technology, 2*(3), 183–189.

[5] Allen, C. (2003). An introduction to heavy-duty diesel engine frictional losses and lubricant properties affecting fuel economy—Part I. *SAE Transactions, 112*(4), 2508–2520.

[6] Becerra Villanueva, J. A., Jimenez, F. J., Torres, M., Sanchez, D. T., & Carvajal, E. (2011). Failure analysis of reciprocating compressor crankshafts. *Engineering Failure Analysis, 18*(2), 735–746. https://doi.org/10.1016/j.engfailanal.2010.12.004

[7] Mateus, J., Anes, V., Galvão, I., & Reis, L. (2019). Failure mode analysis of a 1.9 turbo diesel engine crankshaft. *Engineering Failure Analysis, 101*, 394–406. https://doi.org/10.1016/j.engfailanal.2019.04.004

[8] Pandey, R. K. (2003). Failure of diesel-engine crankshafts. *Engineering Failure Analysis, 10*(2), 165–175. https://doi.org/10.1016/S1350-6307(02)00053-5

[9] Haapakoski, J. (2016). *Medium-speed four-stroke diesel engine cylinder pressure effect on component dimensioning* [Master's thesis, University of Oulu]. University of Oulu Repository. http://urn.fi/URN:NBN:fi:oulu-201612023172

[10] Shiao, Y. J., & Moskwa, J. J. (1993). An investigation of load force and dynamic error magnitude using the lumped mass connecting rod model. *SAE Transactions, 102*(3), 837–846. https://www.jstor.org/stable/44611421

[11] Montazersadgh, F. H., & Fatemi, A. (2007). Dynamic load and stress analysis of a crankshaft. *SAE Technical Paper 2007-01-0258*. https://doi.org/10.4271/2007-01-0258

[12] Montazersadgh, F. H., & Fatemi, A. (2008). Optimization of a forged steel crankshaft subject to dynamic loading. *SAE International Journal of Materials and Manufacturing, 1*(1), 211–217. https://doi.org/10.4271/2008-01-0432

[13] Nikolić, N., Dorić, J., & Jocanović, M. (2016). A computer program for the visualization of IC engine crankshaft main bearings load. In *Proceedings of the 9th International Symposium Konstruisanje-Oblikovanje-Dizajn (KOD)* (pp. 89–92).

[14] Moon, S. M., Cho, Y. J., & Kim, T. W. (2018). Evaluation of lubrication performance of crankpin bearing in a marine diesel engine. *Friction, 6*(3), 1–8. https://doi.org/10.1007/s40544-017-0196-0

[15] Sun, J., Li, B., Zhu, S., Miao, E., Wang, H., Zhao, X., & Teng, Q. (2019). Lubrication performance of connecting-rod and main bearing in different engine operating conditions. *Chinese Journal of Mechanical Engineering, 32*, Article 23. https://doi.org/10.1186/s10033-019-0335-9

[16] Cihan, Ö. (2020). Deformation and stress analysis of crankshafts for single-cylinder and four-cylinder IC engine using ANSYS. *Cumhuriyet Science Journal, 41*(1), 298–304. https://doi.org/10.17776/csj.586687

[17] Sumardiyanto, D., & Susilowati, S. E. (2021). Analysis the occurrence of wear on crankpin bearing in diesel engine. *Journal of Mechanical Engineering and Automation, 10*(1), 19–23. https://doi.org/10.5923/j.jmea.20211001.03

[18] Solangi, E., Memon, I. A., Memon, M. A., Raees, M., & Khan, M. A. (2023). Failure analysis of a diesel engine crankshaft based on finite element modeling. *Journal of Applied Engineering & Technology, 7*(1), 1–9. https://doi.org/10.55447/jaet.07.01.82

[19] Azzawi, M. M., Hadi, A. S., & Abdullah, A. R. (2023). Finite element analysis of crankshaft stress and vibration in internal combustion engines using ANSYS. **Mathematical Modelling of Engineering Problems, 10*(3), 1011–1016. https://doi.org/10.18280/mmep.100335

[20] Yin, J., Zhang, R., Lyu, B., & Meng, X. (2024). Temperature evolution prediction of engine big-end bearing by tribo-dynamics modeling and wireless measurement verification. Tribology International, 194*, Article 109566. https://doi.org/10.1016/j.triboint.2024.109566

[21] Jayanthan, G., Abu Bakar, S. A., & Mazali, I. I. (2024). Fatigue life and stress analysis of a single-cylinder four-stroke crankshaft. *International Journal of Automotive and Mechanical Engineering, 21*(3), 11695–11711. https://doi.org/10.15282/ijame.21.3.2024.19.0902

[22] Chmielowiec, A., Woś, W., & Czyżewski, J. (2025). Numerical analysis of inertia forces in the connecting rod and their impact on stress formation. *Materials, 18*(6), Article 1385. https://doi.org/10.3390/ma18061385

[23] Chen, Y., Liu, X., Wang, X., & Wang, Y. (2024). Speed-based analysis and prediction of fatigue life for the crankshaft via genetic algorithm. *Proceedings of the Institution of Mechanical Engineers, Part D: Journal of Automobile Engineering, 239*(7), 2823–2837. https://doi.org/10.1177/09544070241237318

[24] Liu, Y., Zhu, M., Chen, H., et al. (2026). Fatigue life prediction and optimization design of marine medium-speed diesel engine crankshaft based on Kriging surrogate model. *Journal of the Brazilian Society of Mechanical Sciences and Engineering, 48*, Article 19. https://doi.org/10.1007/s40430-025-06001-1

[25] Ligier, J.-L. (1997). *Lubrification des paliers moteurs*. Éditions Technip.

[26] Zhu, S. (1991). *A dynamic model for automotive diesel engines* [Doctoral dissertation, University of Wisconsin–Madison].

[27] Den Hartog, J. P. (1985). *Mechanical vibrations*. Dover Publications.

[28] Rajendran, S., & Narasimhan, M. V. (1997). Effect of inertia variation due to reciprocating parts and connecting rod on coupled free vibrations of the crankshaft. *Journal of Engineering for Gas Turbines and Power, 119*(1), 257–262. https://doi.org/10.1115/1.2815557

[29] Kevin, H., & Brian, D. (2016). *Vehicular engine design* (2nd ed.). Springer. https://doi.org/10.1007/978-3-7091-1859-7

[30] Starjinski, V. (1984). *Mécanique rationnelle: Cours abrégé adapté au programme complet des écoles supérieures*. Mir-Moscow.

[31] Jensen, E. J. (1970). Crankshaft strength through laboratory testing. *SAE Technical Paper 700526*. Society of Automotive Engineers.

## 7 Conflict of Interest Statement

The authors declare that they have no known competing financial interests or personal relationships that could have appeared to influence the work reported in this paper.

## 8 Author contributions

Djamel Mazari: conceptualization, supervision; Abdelhalim Soussa: methodology, visualization; Khadidja Boualem: writing-original draft preparation, validation, resources; Mustapha Bordjane: investigation, data curation, formal analysis.

## 9 Data availability statement

The data that support the findings of this study are available on request from the corresponding author.

## 10 Supplementary materials

No supplementary material associated with the article.

*Paper submitted: 25.09.2025.*

*Paper accepted: 27.07.2026.*

*This is an open access article distributed under the CC BY 4.0 terms and conditions*